In vivo super-resolution photoacoustic computed tomography by localization of single dyed droplets

Li, Lei, Zhang, Pengfei, Wang, Lihong

Lei Li, Pengfei Zhang, Lihong V. Wang, "In vivo super-resolution photoacoustic computed tomography by localization of single dyed droplets," Proc. SPIE 11240, Photons Plus Ultrasound: Imaging and Sensing 2020, 112402U (17 February 2020); doi: 10.1117/12.2547562

SPIE.

Event: SPIE BiOS, 2020, San Francisco, California, United States

In vivo super-resolution photoacoustic computed tomography by localization of single dyed droplets

Lei Li[a], Pengfei Zhang[b], Lihong V. Wang[a]*
[a]Caltech Optical Imaging Laboratory, Andrew and Peggy Cherng Department of Medical Engineering and Department of Electrical Engineering, California Institute of Technology, 1200 E California Blvd., Pasadena, CA 91125; [b]Present address: School of Precision Instruments and Optoelectronics Engineering, Tianjin University, Tianjin, 300072, China
* Correspondence should be addressed to: LVW@Caltech.edu.

ABSTRACT

The spatial resolution of photoacoustic (PA) computed tomography (PACT) is limited by acoustic diffraction. Here, we report *in vivo* superresolution PACT, which breaks the acoustic diffraction limit by localizing the centers of single dyed droplets. The dyed droplets generate much stronger PA signals than blood and can flow smoothly in blood vessels; thus, they are excellent tracers for localization-based superresolution imaging. The flowing droplets were first localized, and then their center positions were used to construct a superresolution image that exhibits sharper features and more finely resolved vascular details. A 6-fold improvement in spatial resolution has been realized *in vivo*.
Keywords: Photoacoustic computed tomography; super-resolution; localization; single dyed droplets

1. INTRODUCTION

Photoacoustic tomography (PAT) is a nonionizing, hybrid imaging modality that combines optical excitation and acoustic detection, offering high optical contrast, and high spatial resolution at depths inside biological tissues[1, 2]. In PAT, nanosecond-pulsed laser illumination of absorbing molecules generates volume expansion due to the transient local temperature rise. The rapid thermoelastic expansion of the stressed tissue generates acoustic waves that propagate in the tissue—with orders of magnitude weaker scattering than light scattering on a per unit path length basis in the acoustic frequency of interest—and are detected by an ultrasonic transducer or a transducer array.[3-5] PAT inherits the advantage of high optical contrast in optical imaging methods while breaking the optical diffusion limit on penetration of high-resolution optical imaging by detecting ultrasound. PAT can work in both optical ballistic and diffusive regimes, providing multiscale imaging solutions. By scanning a tightly focused laser beam in the optical ballistic regime, a PAT system can provide optical-resolution photoacoustic microscopy (OR-PAM)[6-9]. Recently, OR-PAM has been used for high-speed, high-resolution mapping of the cortical blood vessel network and for studying the hemodynamics in the mouse brain cortex[10]. The penetration depth of OR-PAM is generally limited to ~1–2 mm, because its high spatial resolution depends on the tight optical focus of ballistic photons[11, 12]. Photoacoustic computed tomography (PACT) detects acoustic waves generated by both ballistic and diffused photons and retrieves the optical absorption distribution through an inverse algorithm, allowing high-resolution imaging at a depth up to several centimeters[13-15]. PACT has been used for imaging small-animal whole-body dynamics, functional whole mouse brain hemodynamics, and human breast tumors at high spatiotemporal resolutions[16-20].

However, the resolution of PACT is fundamentally limited by acoustic diffraction, and thus by the acoustic wavelength in tissues. Although finer resolution can be achieved by detecting higher frequency ultrasound, the associated increase in ultrasound attenuation decreases the penetration depth[21, 22]. Inspired by super-resolution fluorescence imaging techniques, such as photoactivation localization microscopy (PALM) [23], several techniques have been exploited to break the acoustic diffraction limit in PACT. One of them utilized the PA signal fluctuations induced either by speckle illumination or by flowing absorbers[24]. More recently, super-resolution PA imaging has also been demonstrated by localization of flowing microbeads[25]. However, none of these techniques has been successfully applied to *in vivo* imaging yet. The disadvantage of the fluctuation-based technique is that the speckle contrast becomes too low to detect in deep tissues, due to the orders of magnitude smaller size of the fully developed speckle grains than the detection acoustic wavelength. Moreover, one of the drawbacks in beads-based-localization technique is that solid beads can jam small blood vessels and block blood flow, impeding *in vivo* applications.

Photons Plus Ultrasound: Imaging and Sensing 2020, edited by Alexander A. Oraevsky, Lihong V. Wang,
Proc. of SPIE Vol. 11240, 112402U · © 2020 SPIE · CCC code: 1605-7422/20/$21 · doi: 10.1117/12.2547562

In this paper, we report a novel technique for *in vivo* super-resolution PACT. This technique breaks the acoustic diffraction limit by localizing flowing dyed droplets[26]. The droplets were prepared by dissolving hydrophobic dye IR-780 iodide in oil, followed by mixing with water. The dyed droplets produce much higher PA signals than the blood background and can flow smoothly in blood vessels. Once injected into the bloodstream, the droplets can be tracked and localized with high precisions on account of their high absorption contrast. The *in vivo* resolution improvement was demonstrated by imaging the cortical layer of a mouse brain during the droplet injection. A super-resolution image built from localization of ~220,000 droplets showed sharper features and resolved finer vascular details. Single droplets were also tracked in the deep brain, and their flow directions and speeds were characterized. The experimental results suggest that the proposed technique is a promising tool for imaging blood capillaries in deep tissues.

2. METHODS

The droplets were prepared by mixing oil-dissolved dye (IR-780) with water. The molar absorption coefficient of the IR-780 iodide dye solution is 300 times higher than that of hemoglobin (80% oxy-hemoglobin and 20% deoxy-hemoglobin) at 780 nm (**Fig. 1a**). Given the normal hemoglobin concentration (150 g/L) in whole blood and the gram-molecular weight of hemoglobin (64,500 g/mole)[27], the absorption coefficient of the dye solution at 2 mM is about 260 times higher than that of the whole blood. Owing to the high contrast, the droplets in the bloodstream are effective tracers. A silicone capillary tube with a 300-μm inner diameter was embedded in 3% agar gel to mimic a blood vessel; we injected whole bovine blood mixed with the droplet suspension with a ratio of 1000:1 into the tube. The concentration of the droplets was controlled so that, statistically, no more than one droplet appeared in an acoustic diffraction-limited volume anytime.

Once injected into the bloodstream, the droplets, flowing through the blood vessels, are tracked by PACT to visualize the vascular network. To track single droplets in vessels by PACT, the time-lapse images were firstly denoised by applying a 2-D adaptive noise-removal filter[28]. Then subtraction of adjacent frames highlighted flowing single droplets. In order to localize the single droplets, the differential grayscale images were converted into binary images by thresholding the pixel values at 1/4 of their maxima. The bright spots within a range of 16 to 64 pixels in the binary images were considered to be the regions containing droplets. Any spots with a roundness less than 0.7 were discarded, which rejected droplet clusters and artifacts. The centroids of the bright spots in the binary images were determined by using the image processing toolbox in Matlab (Mathworks, Inc.), such that the single droplets in the differential grayscale images were coarsely located. Then for each droplet, a region of interest (ROI), centered at its centroid, was isolated from the grayscale images. The ROI with 11 × 11 pixels was fitted with a 2-D Gaussian function, yielding a more precise localization of the droplet. Each droplet was represented by a 2-D Gaussian-distributed spot that was located at its center with a radius equal to its localization uncertainty. By adding up all the droplet images, an image with a spatial resolution beyond the acoustic diffraction limit was obtained. A pixel size of 5 μm was used in the super-resolution image reconstruction.

Single droplets are localized with high precision, and their center positions are used to construct an image with a spatial resolution beyond the acoustic diffraction limit (**Fig. 1b and c**)—a principle widely used in single-molecule localization-based super-resolution fluorescence microscopy and single-microbubble localization-based super-resolution ultrasound imaging[29].

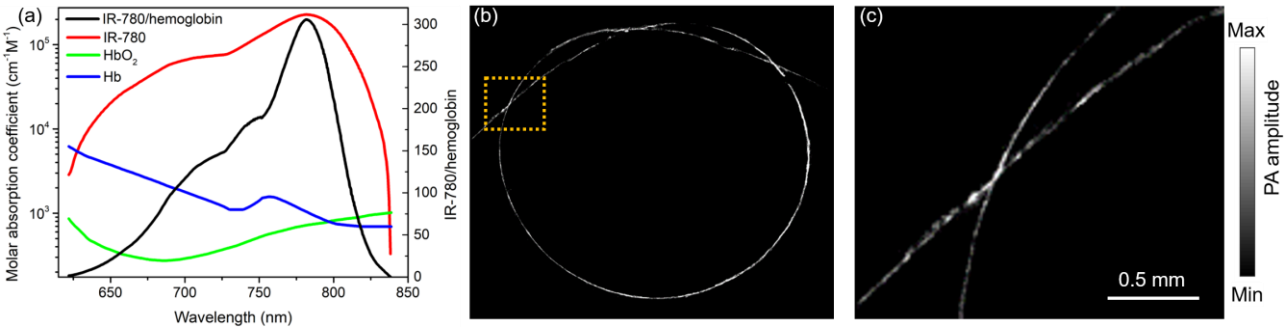

Figure 1. (a) Absorption spectra of oxy-hemoglobin (HbO_2), deoxy-hemoglobin (Hb) and IR-780 dye solution as well as the absorption coefficient ratio of IR-780 to hemoglobin (80% HbO_2 and 20% Hb). (b) Super-resolution PACT image of the tube acquired by localizing single droplets. (c) Zoom-in of (b) in the region indicated by the dashed rectangle.

3. RESULTS

In the *in vivo* study, droplets were used for improving the spatial resolution in PACT of a mouse brain vasculature. The resolution of the conventional PACT system was quantified to be ~150 μm [30]. The mouse brain was firstly imaged using hemoglobin as the endogenous optical contrast. The laser was tuned to 780 nm, and the pulsed energy was set to 100 mJ. The optical fluence on the head surface was 30 mJ/cm^2. The universal back-projection algorithm[31] was used to convert the radio-frequency (RF) data into images. The reconstructed image was shown in **Fig. 2a**. The brain was then continuously imaged while droplets were injected into the heart through the catheter. As mentioned above, the droplet suspension was prepared with 20 μL of the dye solution (2 mM) in 1 mL of water, leading to a droplet concentration of about 4×10^7 mL^{-1}. A 1-mL syringe filled with the suspension was then connected to the catheter by a 25G needle, and the suspension was injected by a syringe pump (EW-74905-52, Cole-Parmer). To maintain the droplet concentration *in vivo*, a 6-second infusion at a pumping speed of 50 μL/min was repeated every 4 minutes until the end of the imaging session. The droplet concentration in the blood was estimated to be 1×10^5 mL^{-1}, basing on the volume of the droplet suspension during each injection cycle (5 μL) and the blood volume in a mouse (~1.5 mL[32]). The number of droplets appeared in an acoustic diffraction-limited volume (150 μm × 150 μm × 500 μm) was thus about 1.25. However, because the PA amplitudes of some small droplets were below the fluctuations in those of the blood background, the number of droplets that were detectable in an acoustic diffraction-limited volume was actually less than one, which allowed tracking and localization of single droplets in the mouse brain. The PACT system started to acquire data approximately 10 seconds after the initial injection, when the injected droplets had been pumped into the brain by the heart. The cortical layer was continuously imaged for half an hour with a frame rate of 20 Hz, resulting in a total of 36,000 frames of images.

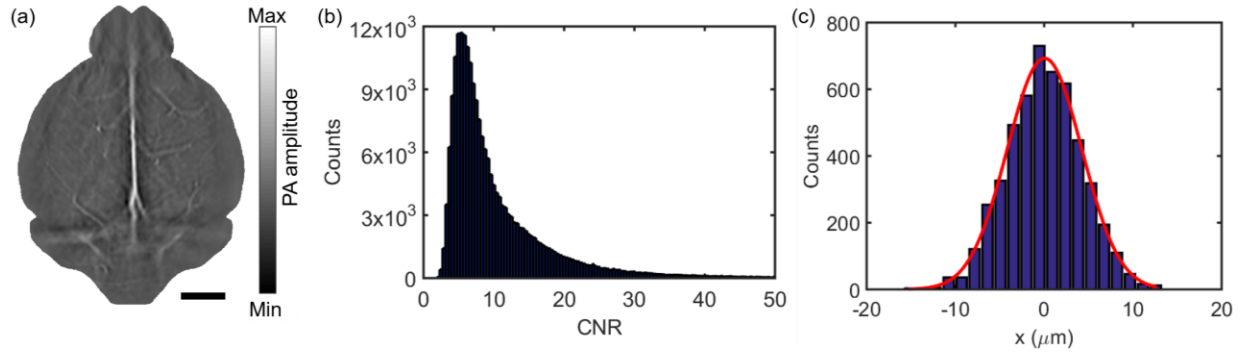

Figure 2. (a) Reconstructed bipolar image of the cortical vasculature of a mouse brain acquired by conventional PACT. The scale bar is 2 mm. (b) Histogram of the experimental CNRs of the droplets. A total of ~220,000 droplets were counted, and a majority of the droplets exhibited CNRs of around 5. (c) Histogram of the localized positions of a droplet simulated with a CNR of 5. A total of 5000 simulations were made, and the droplet center was determined by a 2-D Gaussian fitting. The full width at half maximum (FWHM) of the histogram was determined to be 10 μm in (b). The simulations were performed by assuming that the image of a single droplet has a Gaussian distribution with both of the peak amplitude and the radius close to the typical values as determined in the experiments, and then Gaussian noise was added to give a CNR of 5.

The reconstructed images were denoised and subtracted from the adjacent frames to highlight flowing single droplets. The extracted images of single droplets were then analyzed by 2-D Gaussian fitting, and their centers were determined. The localization precision depended on the contrast-to-noise (CNR) ratio of the droplet. The histogram of the droplets' CNRs shows that a majority of the droplets exhibited CNRs of around 5, and the localization precision was estimated to be 10 μm by numerical simulation (**Fig. 2b and c**).

Figures 3a shows the images of the cortical layer vessels from super-resolution PACT. In the super-resolution image, the vessels appear sharper, and the closely neighboring vessels can be resolved. The droplet-localization technique does not only improve the PACT resolution but also light up the vessels that are otherwise obscured by blood background. The super-resolution image resolves bifurcated vessels with a separation distance of 25 μm. These results suggest that the spatial resolution of PACT has been improved by a factor of 6 by the localization of single droplets.

It should be noted that a few features appearing in the conventional image became invisible in the super-resolution image. The differences of the vascular network in the super-resolution image and the conventional image can be found in the overlaid image (**Fig. 3b**). The artifacts were caused by the limited number of droplets in some vessels and the fact that some features in the conventional image were not blood vessels at all. Moreover, the superior sagittal sinus shows a hollow feature rather than a filled line with Gaussian-distributed cross-section as in the conventional image. An explanation to this artifact might be that dyed droplets flow faster in the central-line of big vessels and slower near the vascular wall[33]. Due to the low frame rate, the slower-moving droplets were easier to track, resulting in more localized droplets near the vascular wall in the super-resolution image. These artifacts can be mitigated by increasing the frame rate in the future.

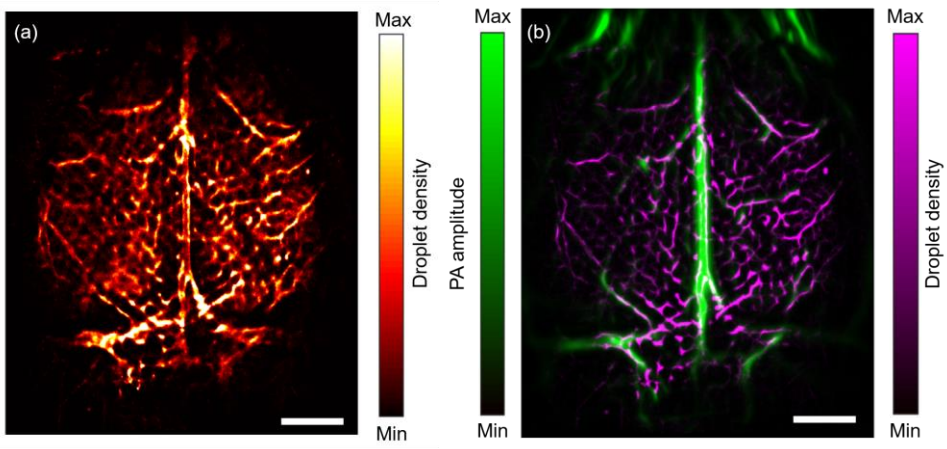

Figure 3. (a) Super-resolution image of the cortical vasculature of the mouse brain constructed from the centers of the localized droplets. The scale bar is 2 mm. (b) An overlay of the super-resolution image (purple) and the conventional image (green). The scale bar is 2 mm.

4. DISCUSSION

In summary, we reported a technique for super-resolution PACT *in vivo*. The technique achieved 25 μm resolution in a live mouse brain, breaking the acoustic diffraction limit by the localization of single flowing droplets in vessels. The droplets were prepared by dissolving hydrophobic dye IR-780 iodide in oil, followed by mixing with water. The dye is highly absorbing at 780 nm, producing much higher PA signals than does blood at this wavelength. Taking advantage of their small sizes and the liquid characteristics, the droplets flowed smoothly in blood vessels, providing significant PA contrast in the bloodstream. The resolution enhancement was demonstrated by continuously imaging the cortical layer of a mouse brain during droplet injection. The droplets flowing in vessels were localized, and their centers were used to construct an image with a resolution finer than the acoustic diffraction limit. Superior to conventional PACT images, the super-resolution PACT images showed sharper features and resolved finer vessels, with the spatial resolution improved by a factor of 6. Single droplets were also trackable in the brain at a depth of 4 mm, as demonstrated by imaging the mouse brain in a coronal plane, and the droplet flow directions and speeds were also characterized in the deep brain.

Droplet-localization PACT can be improved further. Firstly, dyed droplets with higher optical absorption would increase the spatial resolution due to the inverse relationship between the localization precision and the CNR of single droplets[34]. Thus, photoacoustically brighter dye at a longer wavelength (1.0–1.7 μm) would allow super-resolution imaging of vasculature in deeper tissues. Secondly, the sizes of the droplets are dispersed in this work, and many small droplets generated a background in the PACT images, degrading the localization precision. This problem could be circumvented by generating mono-dispersed droplets using a microfluidic device[35]. Thirdly, some droplets displayed moon-like shapes, probably due to their deviation from the focal plane of the transducers, and thus 2-D Gaussian fitting to these images produced a bias in their center estimation. An estimator with less bias is required to process the images of these droplets. Fourthly, the current imaging frame rate is 20 Hz, limited by the laser repetition rate. Although the droplets move slowly in absolute speed (1.3–7.5 mm/s), they move fast on a super-resolution scale, i.e., the droplets displace 1/2 of the super-resolution pixel width (25 μm/2) over a short time interval. To capture the minute displacement accurately, high frame rates are required. Moreover, a high frame rate can also effectively reduce the data acquisition

time and help to remove the artifacts resulted from the limited number of localized droplets. The technique developed in this work is expected to find wide applications in imaging blood vessels and monitoring targeted drug delivery in deep tissues.

This work was sponsored by the NIH grants DP1 EB016986 (NIH Director's Pioneer Award), R01 CA186567 (NIH Director's Transformative Research Award), U01 NS090579 (BRAIN Initiative), and U01 NS099717 (BRAIN Initiative). L.W. has a financial interest in Microphotoacoustics, Inc., CalPACT, LLC, and Union Photoacoustic Technologies, Ltd., which, however, did not support this work. The other authors declare no conflict of interest.

REFERENCES

[1] L. V. Wang, and S. Hu, "Photoacoustic Tomography: In Vivo Imaging from Organelles to Organs," Science, 335(6075), 1458-1462 (2012).
[2] P. C. Beard, "Biomedical photoacoustic imaging," Interface Focus, 1, 602-631 (2011).
[3] L. Li, [Multi-Contrast Photoacoustic Computed Tomography] California Institute of Technology, (2019).
[4] D. Razansky, M. Distel, C. Vinegoni *et al.*, "Multispectral opto-acoustic tomography of deep-seated fluorescent proteins in vivo," Nature Photonics, 3(7), 412-417 (2009).
[5] Y. Li, L. Li, L. Zhu *et al.*, "Snapshot photoacoustic topography through an ergodic relay for high-throughput imaging of optical absorption," Nature Photonics, 1-7 (2020).
[6] L. Zhu, L. Li, L. Gao *et al.*, "Multiview optical resolution photoacoustic microscopy," Optica, 1(4), 217-222 (2014).
[7] L. Li, C. Yeh, S. Hu *et al.*, "Fully motorized optical-resolution photoacoustic microscopy," Optics letters, 39(7), 2117-2120 (2014).
[8] J. Shi, T. T. Wong, Y. He *et al.*, "High-resolution high-contrast mid-infrared imaging of fresh biological samples with ultraviolet-localized photoacoustic microscopy (Conference Presentation)." 10878, 1087825.
[9] H.-C. Hsu, L. Li, J. Yao *et al.*, "Dual-axis illumination for virtually augmenting the detection view of optical-resolution photoacoustic microscopy," Journal of biomedical optics, 23(7), 076001 (2018).
[10] J. Yao, L. Wang, J.-M. Yang *et al.*, "High-speed label-free functional photoacoustic microscopy of mouse brain in action," Nature methods, 12(5), 407 (2015).
[11] T. Imai, J. Shi, T. T. Wong *et al.*, "High-throughput ultraviolet photoacoustic microscopy with multifocal excitation," Journal of biomedical optics, 23(3), 036007 (2018).
[12] Y. He, L. Wang, J. Shi *et al.*, "In vivo label-free photoacoustic flow cytography and on-the-spot laser killing of single circulating melanoma cells," Scientific reports, 6, 39616 (2016).
[13] Z. Wu, L. Li, Y. Yang *et al.*, "A microrobotic system guided by photoacoustic computed tomography for targeted navigation in intestines in vivo," Science Robotics, 4(32), eaax0613 (2019).
[14] T. P. Matthews, J. Poudel, L. Li *et al.*, "Parameterized Joint Reconstruction of the Initial Pressure and Sound Speed Distributions for Photoacoustic Computed Tomography," SIAM Journal on Imaging Sciences, 11(2), 1560-1588 (2018).
[15] B. Rao, R. Zhang, L. Li *et al.*, "Photoacoustic imaging of voltage responses beyond the optical diffusion limit," Scientific reports, 7(1), 2560 (2017).
[16] P. Zhang, L. Li, L. Lin *et al.*, "High‐resolution deep functional imaging of the whole mouse brain by photoacoustic computed tomography in vivo," Journal of biophotonics, 11(1), e201700024 (2018).
[17] M. Toi, Y. Asao, Y. Matsumoto *et al.*, "Visualization of tumor-related blood vessels in human breast by photoacoustic imaging system with a hemispherical detector array," Scientific reports, 7, 41970 (2017).
[18] J. Yao, A. A. Kaberniuk, L. Li *et al.*, "Multiscale photoacoustic tomography using reversibly switchable bacterial phytochrome as a near-infrared photochromic probe," Nature methods, 13(1), 67 (2016).
[19] C. Yeh, L. Li, L. Zhu *et al.*, "Dry coupling for whole-body small-animal photoacoustic computed tomography," Journal of biomedical optics, 22(4), 041017 (2017).
[20] Y. Qu, L. Li, Y. Shen *et al.*, "Dichroism-sensitive photoacoustic computed tomography," Optica, 5(4), 495-501 (2018).
[21] L. V. Wang, "Multiscale photoacoustic microscopy and computed tomography," Nature Photonics, 3, 503 (2009).

[22] L. Li, A. A. Shemetov, M. Baloban *et al.*, "Small near-infrared photochromic protein for photoacoustic multi-contrast imaging and detection of protein interactions in vivo," Nature communications, 9(1), 2734 (2018).
[23] E. Betzig, G. H. Patterson, R. Sougrat *et al.*, "Imaging Intracellular Fluorescent Proteins at Nanometer Resolution," Science, 313(5793), 1642-1645 (2006).
[24] T. Chaigne, B. Arnal, S. Vilov *et al.*, "Super-resolution photoacoustic imaging via flow-induced absorption fluctuations," Optica, 4(11), 1397-1404 (2017).
[25] X. L. Dean-Ben, and D. Razansky, "Localization optoacoustic tomography," Light: Science & Applications, 7, 18004 (2018).
[26] P. Zhang, L. Li, L. Lin *et al.*, "In vivo superresolution photoacoustic computed tomography by localization of single dyed droplets," Light: Science & Applications, 8(1), 36 (2019).
[27] S. Prahl, [Optical Absorption of Hemoglobin].
[28] J. S. Lim, [Two-dimensional signal and image processing] Prentice Hall, Englewood Cliffs, NJ, 710 (1990).
[29] C. Errico, J. Pierre, S. Pezet *et al.*, "Ultrafast ultrasound localization microscopy for deep super-resolution vascular imaging," Nature, 527, 499 (2015).
[30] L. Li, L. Zhu, C. Ma *et al.*, "Single-impulse panoramic photoacoustic computed tomography of small-animal whole-body dynamics at high spatiotemporal resolution," Nature biomedical engineering, 1(5), 0071 (2017).
[31] M. Xu, and L. V. Wang, "Universal back-projection algorithm for photoacoustic computed tomography," Physical Review E, 71(1), 016706 (2005).
[32] A. C. Riches, J. G. Sharp, D. B. Thomas *et al.*, "Blood volume determination in the mouse," The Journal of physiology, 228(2), 279-284 (1973).
[33] L. Li, C. Yeh, S. Hu *et al.*, "Fully motorized optical-resolution photoacoustic microscopy," Optics Letters, 39(7), 2117-2120 (2014).
[34] R. E. Thompson, D. R. Larson, and W. W. Webb, "Precise Nanometer Localization Analysis for Individual Fluorescent Probes," Biophysical Journal, 82(5), 2775-2783 (2002).
[35] L. Yobas, S. Martens, W.-L. Ong *et al.*, "High-performance flow-focusing geometry for spontaneous generation of monodispersed droplets," Lab on a Chip, 6(8), 1073-1079 (2006).